Partial cross sections of the ^{92}Mo(p,γ) reaction and the γ strength in ^{93}Tc

J. Mayer,[1,*] S. Goriely,[2] L. Netterdon,[1] S. Péru,[3] P. Scholz,[1] R. Schwengner,[4] and A. Zilges[1]

[1]*Institute for Nuclear Physics, University of Cologne, Zülpicher Str. 77, 50937 Cologne, Germany*
[2]*Institut d'Astronomie et d'Astrophysique, Université Libre de Bruxelles, CP226, 1050 Brussels, Belgium*
[3]*CEA, DAM, DIF, F-91297 Arpajon, France*
[4]*Helmholtz-Zentrum Dresden-Rossendorf, 01328 Dresden, Germany*

Background: ^{92}Mo is the most abundant nucleus of the p nuclei, with an isotopic abundance of more than 14 %. The γ-process nucleosynthesis is believed to produce ^{92}Mo but fails to explain its large abundance, especially with respect to the other p nuclei produced in the same stellar environment. Further studies require precise nuclear models for the calculation of reaction cross sections.

Purpose: A measurement of the total and partial cross sections of the ^{92}Mo(p,γ)^{93}Tc reaction allows for a stringent test of statistical-model predictions. Not only different proton + nucleus optical model potentials, but also the γ-ray strength function of ^{93}Tc can be investigated. In addition, high-resolution in-beam γ-ray spectroscopy enables the determination of new precise nuclear structure data for ^{93}Tc.

Method: Total and partial cross-section values were measured by using the in-beam method. Prompt γ rays emitted during the irradiation of ^{92}Mo with protons at seven different energies between 3.7 and 5.3 MeV were detected by using the high-purity germanium (HPGe) detector array HORUS at the Institute for Nuclear Physics, University of Cologne. The $\gamma\gamma$-coincidence method was applied to correlate γ-ray cascades in ^{93}Tc with their origin in the ^{92}Mo + p compound state.

Results: The measured cross sections are compared to Hauser–Feshbach calculations by using the statistical-model code TALYS on the basis of different nuclear physics input models. Using default settings based on standard phenomenological models, the experimental values cannot be reproduced. A shell-model calculation was carried out to predict the low-energy $M1$ strength in ^{93}Tc. Together with Gogny–Hartree–Fock–Bogoliubov (Gogny-HFB) or Skyrme-HFB plus quasi-particle random-phase approximation (QRPA) models for the γ-ray strength function, the agreement between experimental data and theoretical predictions could be significantly improved. In addition, deviations from the adopted level scheme were found.

Conclusions: By using Gogny- or Skyrme-HFB + QRPA $E1$ and shell-model $M1$ strength functions, statistical-model predictions can be significantly improved. Partial cross sections provide a valuable testing ground for γ-ray strength functions for nuclear astrophysics applications. In addition, they can be used to investigate nuclear-structure properties of the compound nucleus.

I. INTRODUCTION

About 35 neutron deficient, stable nuclei cannot be produced by the slow and rapid neutron capture processes [1]. These isotopes are referred to as p nuclei and are believed to be produced by a various set of reactions gathered under the term "p process". Except for four isotopes (^{92,94}Mo, ^{96}Ru, ^{144}Sm), their isotopic abundance is below 2% [2]. Out of all p nuclei, ^{92}Mo stands out with the highest natural abundance of 14.5% ± 0.3%. This has naturally attracted a lot of attention to its production sites and mechanisms [1]. Moreover, ^{92}Mo as well as several other p nuclei with masses $A < 100$ tend to be underproduced in reaction-network calculations for the most likely p-process site—the O/Ne-layer during core-collapse supernovae. Contributions by production mechanisms in the proton-rich neutrino-driven wind of type-II supernova have been proposed, but seem to be ruled out by the constraining measured ratio of ^{92}Nb /^{92}Mo in the Solar System [3,4], leaving the production through a series of (γ,n), (γ,p), and (γ,α) reactions as well as subsequent β decays

in type-II [1,4,5] and type-Ia [6–8] supernovae as the most probable main contributors.

In network calculations, several thousands of nuclei and reactions are involved. Because most nuclei are unstable, reaction rates and cross sections cannot be measured effectively and have to be calculated by using theoretical approaches within the scope of the Hauser–Feshbach statistical model [9]. The predicted cross sections vary vastly depending on the nuclear physics input. Cross-section measurements in nuclear astrophysics aim at constraining the nuclear physics parameters that enter such predictions.

Among all the reactions of interest, the photoproton emission along the magic numbers is known to be an active reaction channel during the p-process flow [1]. The (γ,p) reaction is usually studied through the reverse-radiative proton-capture channel by applying the detailed balance relations between inverse astrophysical rates. The present study focuses on the ^{92}Mo(p,γ)^{93}Tc reaction, which can constrain the reverse ^{93}Tc(γ,p)^{92}Mo production channel of ^{92}Mo during the p process. In addition, it provides sensitive information on the proton + nucleus optical potential and γ-ray strength function of particular relevance in reaction modeling.

---

*jan.mayer@ikp.uni-koeln.de

The reaction cross section has been measured before by means of the activation method with thick [10,11] and thin targets [12]. In all cases, a fluctuating cross section was found at the lowest measured energies, which is an uncommon feature in this type of measurement and cannot be described by using a statistical-model approach. In addition to the total ^{92}Mo(p,γ)^{93}Tc reaction cross section, we present here the first measurements of the partial cross sections to numerous low-lying excited states in ^{93}Tc. Such additional information provides deep insight and model constraints on the electromagnetic deexcitation channels at various excitation energies, as already described in Ref. [13] for the ^{89}Y(p,γ)^{90}Zr reaction and the ^{90}Zr γ-ray strength. In addition, the residual nucleus ^{93}Tc is also interesting from a nuclear structure point of view, in particular for its high spin states [14] and parity violation [15].

In Sec. II, the experiment is described, including the target properties, the experimental setup and the detector efficiency. The data analysis procedure is presented in Sec. III. In Sec. III E, the experimental cross sections are compared with statistical-model calculations, both for production of the ground and metastable state as well as partial cross sections. Finally, conclusions are drawn in Sec. V.

II. EXPERIMENT

The ^{92}Mo(p,γ)^{93}Tc reaction with a Q value of (4086.5 ± 1.0) keV [16] was investigated via in-beam γ-ray spectroscopy with high-purity germanium (HPGe) detectors. Total and partial cross sections were measured at seven different proton energies from 3.7 to 5.3 MeV.

A. Target properties

Metallic molybdenum enriched to 94.1% in ^{92}Mo was used to produce four self supporting targets. Thickness measurements were carried out by applying Rutherford backscattering spectrometry (RBS) [17] prior to the experiment at the RUBION RBS facility of the University of Bochum as well as during the experiment. An excellent description of the measured spectra was obtained by using the RBS simulation software SIMNRA [18], when including surface roughness by means of a thickness distribution [19], see Fig. 1. Areal particle densities in ^{92}Mo varied from (440 ± 30) μcm^{-2} to (700 ± 70) μcm^{-2} for the thinnest and thickest foil, respectively. No deterioration of target material was observed during the experiment. For these foils, the energy loss for protons according to SRIM [20] is between 20 and 34 keV, depending on target thickness and beam energy.

B. Experimental setup

The experiment was performed at the 10 MV FN tandem accelerator of the University of Cologne, Germany. Proton beams with currents between 50 and 350 nA impinged on the aforementioned molybdenum foils mounted together with a thick gold backing ($\approx$150 mg/cm^2) used to stop the beam. The beam energy was calibrated by using the $E_p = 3674.4$ keV resonance of the ^{27}Al(p,γ)^{28}Si reaction [21,22]. The beam current was separately collected and recorded every second
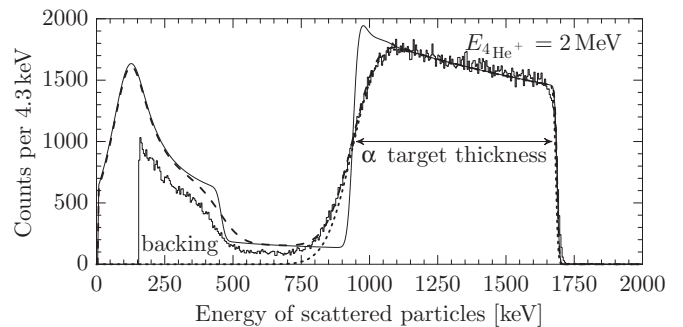

FIG. 1. RBS spectrum for a molybdenum foil. Experimental data were taken at RUBION (Bochum, Germany) by using a 2 MeV ^{4}He$^+$ beam. Areal particle densities can be obtained by simulating the spectra with SIMNRA [18] (solid line). An excellent reproduction was obtained for all targets when accounting for thickness distributions (dashed line). A simulation without the aluminum alloy backing (dotted line) shows negligible influence on the target-thickness determination.

for target, chamber, and cup. To prevent δ electrons from leaving the chamber, a suppression voltage of $U = -400$ V was applied to an aperture at the entrance of the chamber.

The HPGe detector array HORUS was used for prompt γ-ray detection with a setup specifically designed for nuclear astrophysics experiments [22]. Thirteen HPGe detectors, six of which were equipped with bismuth-germanate-type (BGO-type) anti-Compton shields, were mounted at five angles with respect to the beam axis. Pre-amplified signals from the HPGe and RBS detectors were processed by using the digital gamma finder modules (DGF-4C Rev. F) by XIA Inc. [23]. Energy, timing, and veto information was stored in an event-by-event listmode format, which allows for an offline analysis of $\gamma\gamma$ coincidences and active Compton suppression.

C. Detector efficiency

Precise knowledge of the full energy peak (FEP) efficiency for γ rays up to 9.4 MeV is required for the determination of total as well as partial cross sections. In the present case, single (SEP) and double (DEP) escape-peak efficiencies are also required for some partial cross sections to avoid misinterpretation of the data, because the energy distance between some levels in ^{93}Tc is about 511 or 1022 keV.

A point-like ^{226}Ra standard source with known activity and a ^{56}Co source were used to cover energies up to 3.5 MeV [24]. In addition, the aforementioned ^{27}Al(p,γ) resonance was used to produce γ rays with energies of 8.2 and 10.5 MeV [21]. A new GEANT4 [25]-based Monte Carlo simulation was developed to simulate escape-peak efficiencies including active signal vetoing from the BGO-type anti-Compton shields. A good agreement with the experimental data was obtained for all detectors, as shown in Fig. 2. Note that an active veto reduces the escape-peak efficiency by a significant amount. This is beneficial to the experiment, because the fraction of FEP to SEP events increases.
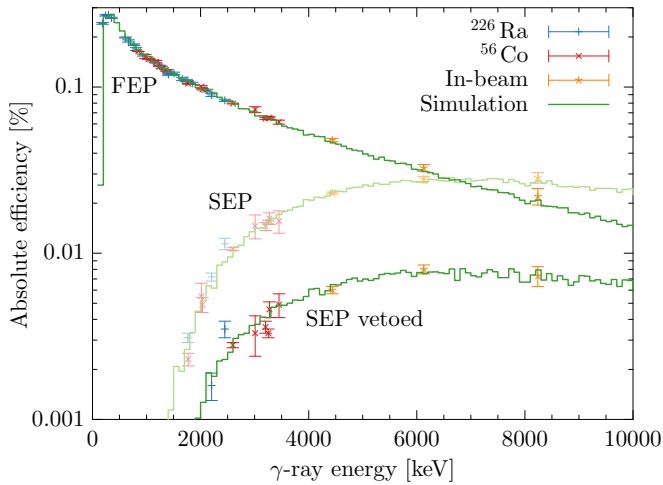
FIG. 2. Full energy peak (FEP) and single escape-peak (SEP) efficiency for one HORUS HPGe detector. Experimental data have been obtained from standard sources and in-beam reactions [^{27}Al(p,γ)^{28}Si, ^{12}C($p,p'\gamma$), ^{19}F(p,α)^{16}O], with the last two scaled to the FEP efficiency. The simulations were carried out by using GEANT4 [25]. It was not necessary to scale the simulated data to match the experimental results. The detector is equipped with a BGO anti-Compton shield whose active veto signal can be used on an event-by-event basis to suppress escape peaks (SEP vetoed).

III. DATA ANALYSIS

A. Production of the compound nucleus

Under the bombardment with projectiles, a capture reaction can occur, forming a highly excited compound nucleus at an energy E_X equal to the sum of the Q value and center-of-mass energy. A spread in excitation energy exists due to an initial spread in beam energy and energy loss in the target. The excited compound state can decay via several paths, resulting in a huge amount of different γ rays. By using HPGe detectors, these can be detected individually. By evaluating all transitions directly deexciting the compound state will give the number of produced nuclei. In most cases, however, it will be more effective to measure all γ rays populating the ground state instead, because the detection efficiency is higher at lower energies. This is only equivalent if the produced isotope has no long-lived metastable state, internal conversions not emitting γ rays, or branching to other isotopes.

The reaction product ^{93}Tc studied in this experiment possesses all of the above. This provides additional challenges in the analysis, which will be discussed in the following.

B. Total-cross-section determination

The metastable state in ^{93}Tc at 391.8 keV has a half live of 43.5 min [26]. Thus, data recorded from start to stop of the irradiation would miss transitions from the metastable state. In addition, the metastable state has a significant electron-capture branching of 22.6 % to ^{93}Mo [26], and the internal decay to the ground state does not necessarily emit a γ ray.

A solution is the individual determination of the production cross sections for the ground and metastable states, which implies determining the ground-state population without the

TABLE I. γ-ray transitions used for cross-section determination. The γ-ray transition at 392 keV is ignored and the 1016 keV γ-ray transition is replaced by γ-ray transitions to the level at 1407.8 keV, as discussed in Sec. III B 1.

	E_f [keV]	γ-ray transitions [keV]
σ_{gs}	0.0	<u>391.8</u>, 680.6, 1194.1, 1434.4, 1515.8, 1801.4, 2257.7, 2338.7, γ_0
σ_m	391.8	<u>1015.9</u>, 1111.2, 1396.2, 2039.1, γ_1
	1407.8	561.2, 725.9, 1023.0, γ_5

contribution of the metastable state, which in the following is called σ_{gs}, effectively ignoring the 392 keV peak. This peak holds all information about the population of the metastable state σ_m, as will be discussed later. The total cross section σ_{tot} can then be determined by adding σ_{gs} to σ_m.

1. Angular distributions

In contrast to radiation emitted from a source, the γ rays from the proton-capture reaction have a nonisotropic angular distribution with respect to the beam axis. Detector yields including efficiency and dead time for each angle θ relative to the beam axis are evaluated and the distribution is fit by using a function of type

$$Y(\theta) = a_0[1 + a_2 P_2(\cos\theta) + a_4 P_4(\cos\theta)], \quad (1)$$

where P_2 and P_4 are the Legendre polynomials of order two and four, respectively. The number of reactions is then given by the sum over all transitions $N_f = \sum a_0$ for the specific final level f. A list of all transitions used is given in Table I. Finally, the cross sections are obtained by normalizing the number of reactions to the number N_p of projectiles and the areal particle density N_T of the target:

$$\sigma_f = \frac{N_f}{N_p N_T}. \quad (2)$$

One transition populating the metastable state at 391.8 keV stems from a level at 1407.8 keV. This state decays solely by emitting a γ ray with an energy of 1015.9 keV [26], which is very close to a transition in ^{27}Al at 1014.5 keV. The latter γ-ray transition is also visible in the spectrum taken only with the backing, thus the γ-ray transition populating ^{93}Tc^m cannot be used for cross-section determination. However, analyzing all γ-ray transitions populating this state gives an equivalent result.

2. Target activity analysis

The cross section for the metastable state can also be obtained by observing its decay during irradiation. In the following, the activation-curve method will be discussed.

Starting with a nonradioactive target, the metastable state is populated by radiative proton-capture reactions and the number of ^{93}Tc^m nuclei will increase with

$$\dot{N}(t) = \sigma \dot{N}_P(t) N_T, \quad (3)$$

where $\dot{N}_P$ is the proton current and N_T is the areal density of the target atoms. At the same time, the number of nuclei decreases by decay,

$$\dot{N}(t) = -\lambda N(t), \tag{4}$$

where λ is the decay constant. The combination of production and decay yields a differential equation which can be solved for constant production by assuming constant projectile current $\dot{N}_P(t)$, yielding the activation equation

$$N(t) = \sigma \dot{N}_P N_T (1 - e^{-\lambda t})/\lambda. \tag{5}$$

However, the projectile current is not constant in an accelerator-based experiment because of natural variation in the source and manual changes. This is corrected by integrating the current over M small time steps Δt:

$$N(M) = \sigma N_T \frac{1 - e^{-\lambda \Delta t}}{\lambda} \sum_{k=1}^{M} \dot{N}_P(k) e^{-\lambda(M-k)\Delta t} \tag{6}$$

$$\approx \sigma N_T \sum_{k=1}^{M} (\dot{N}_P(k)\Delta t) e^{-\lambda(M-k)\Delta t} \tag{7}$$

$$= \sigma N_T \sum_{k=1}^{M} N_P(k)(e^{-\lambda \Delta t})^{M-k} \tag{8}$$

$$= \sigma N_T N_p^{\text{eff}}(M), \tag{9}$$

where $N_p(k)$ is the number of projectiles collected during the kth time step of the complete measurement time $t = M\Delta t$, and N_P^{eff} is the effective number of particles, defined here as

$$N_p^{\text{eff}}(M) = \sum_{k=1}^{M} N_P(k)(e^{-\lambda \Delta t})^{M-k}. \tag{10}$$

In a typical activation experiment, this is only evaluated once at the end of the irradiation. Here, every 10 min a new sub-run is used to record the data. Thus it is possible to evaluate the peak yield $Y_i(M)$ from every new sub-run, thus obtaining an activation curve:

$$Y_i(M) = I_i \lambda N(M) \Delta t, \tag{11}$$

where I_i is the absolute intensity of the γ-ray transition. Thus one can conclude

$$N(M) = \sigma N_T N_p^{\text{eff}}(M) \stackrel{!}{=} \frac{Y_i(M)}{I_i \lambda \Delta t}, \tag{12}$$

$$\Rightarrow Y_i(M) = \underbrace{I_i \lambda \Delta t \sigma N_T}_{c_i} N_p^{\text{eff}}(M). \tag{13}$$

Activation curves for the decay of the metastable state could be obtained, to which the calculated curve $N_p^{\text{eff}}(M)$ was fit via the single parameter c_i (Fig. 3). From this parameter, the cross section

$$\sigma = \frac{c_i}{I_i \lambda \Delta t N_T} \tag{14}$$
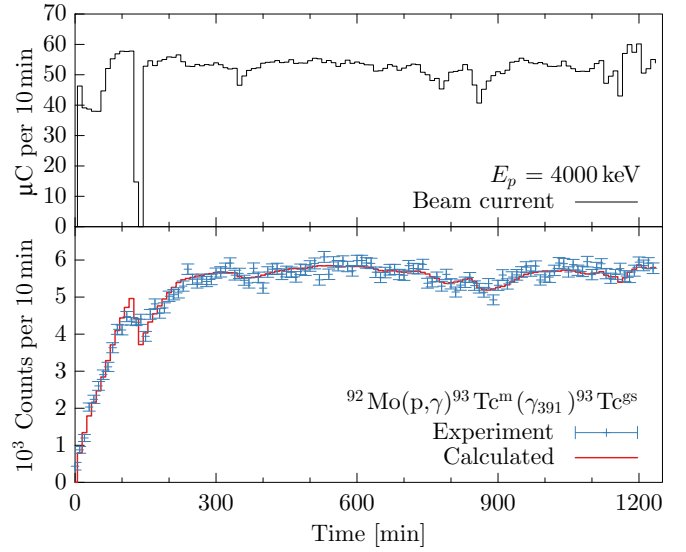
can be finally determined.

FIG. 3. Beam current (top) and resulting $^{93}\text{Tc}^m$ activity (bottom) in time steps of 10 min. The shape of the activation curve is given by the time-dependent beam current and the half-life of the metastable state; see Sec. III B 2. This shape is fit to the experimental yield curve via a single parameter, from which the cross section σ_m can be obtained.

C. Partial cross sections

γ-ray transitions from the decay of the compound state populating states up to the 13th excited level of ^{93}Tc were observed. Partial cross sections could be obtained up to the 11th excited level by evaluating their individual angular distributions, similar to the determination of the total-cross-section values. Because some levels are very close in energy, for some γ-ray transitions, combined cross sections are given. Due to the width of the compound state and the resulting width of the peak, the associated γ-ray transitions could not be resolved. In addition, the energy difference between some states is about 511 or 1022 keV, respectively (see Fig. 4); thus, single- and double-escape-peak efficiencies were utilized to deconvolute the affected peaks.

Note that the γ-ray transition γ_9 populates a level at 1555 keV, which has no known γ decay according to Ref. [26]. This motivated a $\gamma\gamma$-coincidence analysis, which is discussed below.

D. $\gamma\gamma$ coincidences

Prompt γ-ray transitions depopulating the compound state excite specific states in ^{93}Tc, which then further decay to lower-lying states. γ rays emitted in this cascade are observed and recorded together by the detection system. So-called gated spectra can be obtained from this raw data by requiring a coincidence with a second transition. These spectra contain only transitions in coincidence with the gating transition.

At a proton energy of 5100 keV, a sufficient amount of data for a $\gamma\gamma$-coincidence analysis were obtained. The raw listmode data format, containing events with up to 13 HPGe-detector hits, was further processed: Each hit combination in each event was analyzed and, depending
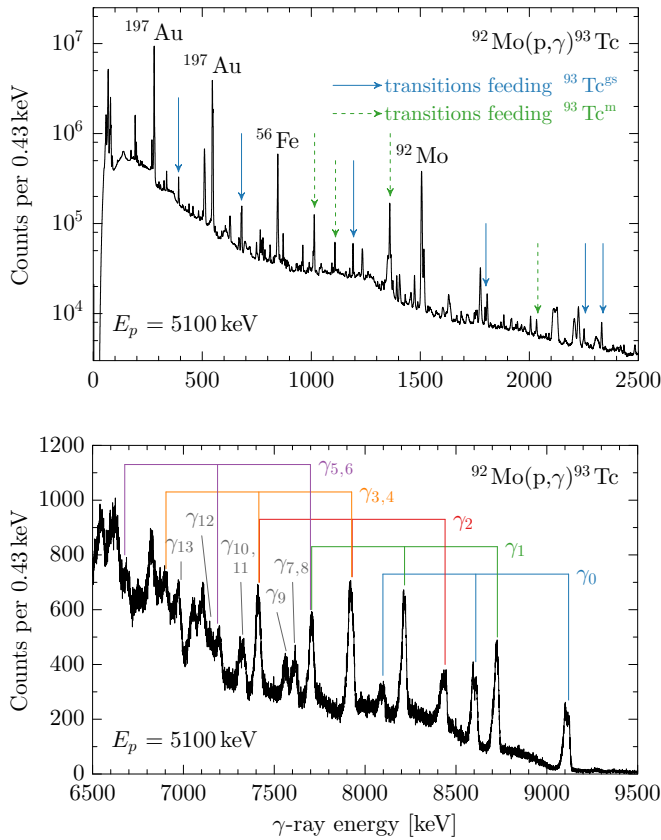
FIG. 4. Typical γ-ray spectrum for the ^{92}Mo(p,γ)^{93}Tc reaction. Detailed view of the low- (top) and high-energy part (bottom). Some strong transitions in the low-energy part stem, as expected, from Coulomb excitation of the gold backing and the target material itself. Transitions feeding the ground and first-excited state of ^{93}Tc are clearly visible. Transitions from the compound state are very prominent in the high-energy part; however, some overlap between full energy and escape peaks is apparent. The spread in excitation energy is the main contribution to the width of the high-energy peaks.

on the time difference between the hits, sorted into $\gamma\gamma$ matrices (two-dimensional histograms). The time-difference spectra show a distinct peak of prompt (causal) coincidences on a flat random-coincidence plateau. Subtracting a matrix containing only random coincidences from a causal- + random-coincidence matrix provides a significant background reduction [27]. Additional background reduction was accomplished by subtracting coincidences close to the peak of interest.

Gating on peaks from transitions depopulating the compound state resulted in almost-flat spectra for γ_0 and γ_1 (not shown) and spectra with very good peak-to-background ratios for γ_2–γ_{11}; see Fig. 5. For the reasons discussed in Sec. III C, some spectra contain peaks from several states or 511 keV annihilation photons.

While the $\gamma\gamma$-coincidence analysis confirms the adopted level scheme [26] to a large extent, striking differences were found for some states:

(i) No evidence was found for the existence of the fourth state at (1190 ± 9) keV ($\frac{1}{2}^-$, $\frac{3}{2}^-$), which has
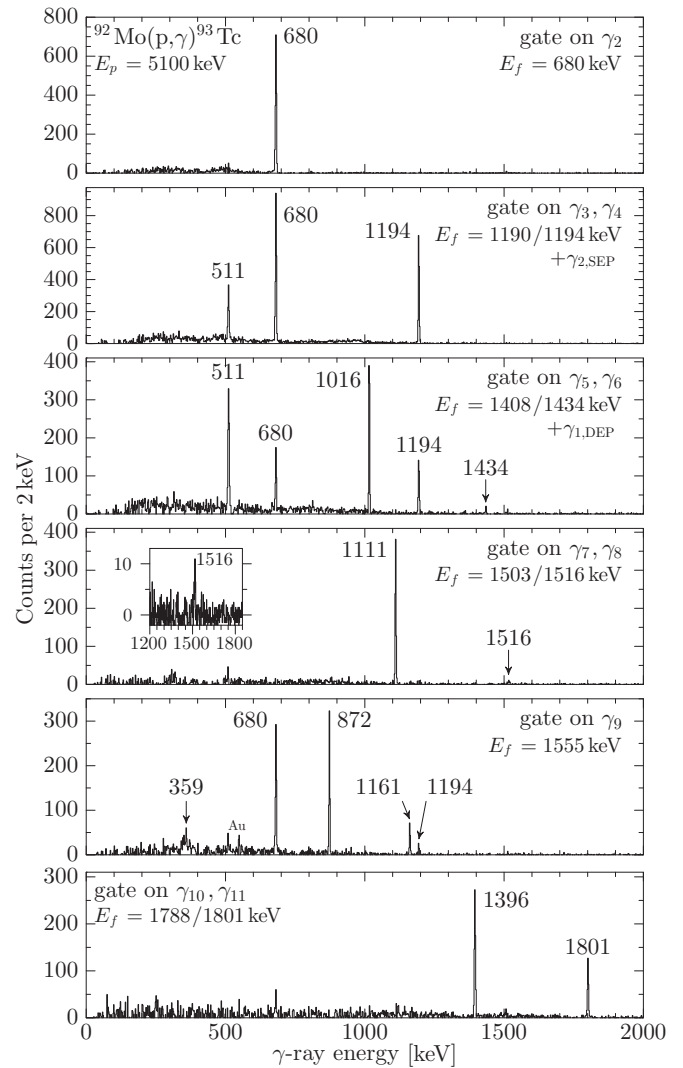

FIG. 5. Coincidence spectra obtained by gating on prompt γ-ray transitions feeding specific levels in ^{93}Tc from the compound state. No evidence for the existence of the (1190 ± 9) keV state was found. Additionally, the population and decay of the 1516 keV state seems very small. In contrast, the decay of the 9th level at (1555 ± 2) keV could be observed with high statistics and previously unknown γ-ray transitions are visible.

been adopted to account for inconsistencies between spectroscopy and ^{93}Ru(ϵ) data for the fifth state at (1194.13 ± 0.10) keV ($\geqslant\frac{7}{2}$); see ENSDF notices for details [26]. For the current spin assignments, a γ-ray transition from the fourth- to the first-excited level should be probable.

(ii) The yield for the decay of the level at (1515.95 ± 0.11) keV in coincidence with the combined population of the 1503 and 1516 keV states was surprisingly small, even though TALYS calculations (see Sec. IV) show a noticeable strength of the γ_8 transition. In addition, the 836 keV γ-ray branching was not visible in coincidence with the 680 keV transition to the ground state.

(iii) The γ-rays peaks at 680 and 1194 keV observed in the gated spectra for γ_5, γ_6 are not expected and suggest unobserved transitions. A gate on the 1194 keV γ-ray transition revealed a small peak at 213 keV, which would match a branching of the 1407 keV state. The existence of the 680 keV peak could be explained by a transition from the 1194 keV state at 513 keV, which would be inseparable from the 511 keV annihilation peak.

(iv) For the 9th state at (1555 ± 2) keV, neither spin nor γ-ray transitions are known. In this experiment, the population of this state from the compound state as well as several decay paths were clearly visible; see Fig. 5. In particular, new γ-ray transitions at (1161 ± 1), (873 ± 1), and (359 ± 1) keV were found in coincidence with the population, which match well to known excited states (Fig. 6). From this, a level energy of (1553 ± 1) keV can be deduced. The branching ratios are given in Table II.
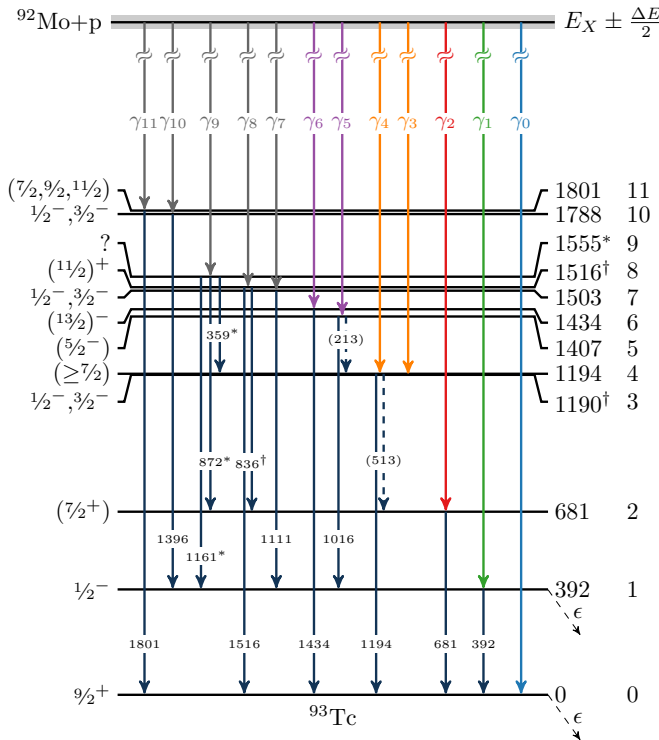
TABLE II. Branching ratios for the deexcitation of the 1553(1) state found by gating on the γ_9 transition for a proton energy of 5100 keV. Energies E_f of the final levels are taken from [26].

E_i [keV]	E_f [keV]	E_γ [keV]	I_γ
1553(1)	391.84	1161(1)	27(5)
1553(1)	680.59	873(1)	100(15)
1553(1)	1194.13	359(1)	21(8)

E. Cross-section results

Production cross sections for the ground and metastable states are given in Table III, and partial cross sections are given in Table IV.

Cross-section values for the production of the metastable state were also be obtained by using the activation-curve method for the internal 392 keV transition, which are systematically $20\% \pm 9\%$ to $57\% \pm 12\%$ higher. With respect to the work-around required for the aluminum contamination in combination with the imperfect level scheme, an incomplete cross-section measurement with the in-beam method is possible.

In comparison with the previous measurements by Sauter and Käppeler [10], Gyürky *et al.* [11], and Hasper *et al.* [12], no fluctuations in the cross sections for the ground and metastable states were found for neighboring energies. This indicates that the level density in the energy range covered in this experiment is high enough for a statistical-model analysis.

IV. STATISTICAL-MODEL CALCULATIONS

Cross sections can show a diverse dependence on different widths. Varying the input channel widths Γ for statistical-model calculations reveals the sensitivity

$$ s = \frac{\Delta\sigma/\sigma}{\Delta\Gamma/\Gamma} \tag{15} $$

of the cross section σ with respect to changes of given input parameters. The ^{92}Mo$(p,\gamma)^{93}$Tc cross section is sensitive to both the proton and photon channel within the measured proton energy range, as shown in Fig. 7. The energy range of astrophysical interest is located from 1.6 to 3.6 MeV for incident protons, corresponding to energies within the Gamow

FIG. 6. Level scheme of ^{93}Tc up to 1.9 MeV. For all unmarked states and transitions, the adopted ENSDF values could be verified in this experiment [26]. Using $\gamma\gamma$ coincidences with a gate on γ_9, previously unknown transitions marked with an asterisk could be identified and the level energy rendered more precisely to (1553 ± 1) keV. In contrast, no evidence for the proposed state at 1190 keV was found. Furthermore, an expected γ ray from the 1516 keV state, marked with a dagger, was neither found in coincidence with the populating γ_8 transition nor with further decay in case of the γ-ray transition to the 680 keV state, probably due to very small population. The 1194 and 680 keV peaks observed in the gated spectra for γ_5, γ_6 suggest transitions at 513 and 213 keV, indicated by dashed arrows.

TABLE III. Cross sections for the ^{92}Mo$(p,\gamma)^{93}$Tc^{gs,m} reaction measured in this experiment. The production cross section of the metastable state was determined by using the in-beam (IB) method and via the activation curve of the internal 392 keV transition (AC392).

E_p [keV]	σ_{gs} [μb]	σ_m [μb] (IB)	σ_m [μb] (AC392)
3672 ± 4	148 ± 12	131 ± 10	170 ± 14
3970 ± 5	251 ± 14	196 ± 10	234 ± 14
4270 ± 5	373 ± 20	243 ± 12	303 ± 18
4566 ± 5	587 ± 65	342 ± 37	476 ± 53
4870 ± 5	810 ± 65	471 ± 36	652 ± 54
5066 ± 5	907 ± 99	510 ± 55	678 ± 76
5273 ± 5	922 ± 49	518 ± 26	815 ± 47

TABLE IV. Experimental partial cross sections for the ^{92}Mo(p,γ) reaction as a function of proton energy E_p. The compound state created by proton capture can decay to different levels in ^{93}Tc emitting γ rays, which are denoted by the number γ_i and energy of the final level E_f, in keV. For some levels, individual γ-ray transitions cannot be separated due to small differences in energy.

E_p [keV]	σ_{γ_0} [μb] 0	σ_{γ_1} [μb] 392	σ_{γ_2} [μb] 680	$\sigma_{\gamma_{3,4}}$ [μb] 1190, 1194	$\sigma_{\gamma_5}, \sigma_{\gamma_6}$ [μb] 1407, 1434	$\sigma_{\gamma_7}, \sigma_{\gamma_8}$ [μb] 1503, 1516	σ_{γ_9} [μb] 1555	$\sigma_{\gamma_{10}}, \sigma_{\gamma_{11}}$ [μb] 1788, 1801
3672(4)	13.2(12)	36.7(35)	8.5(9)	12.1(16)	7.6(14)	11.0(10)	9.5(09)	15.5(15)
3970(5)	22.5(16)	29.9(22)	24.9(17)	9.2(16)	27.0(22)			19.4(14)
4270(5)	35.5(27)	40.1(29)	42.6(30)	10.5(27)	30.0(26)			
4566(5)	52.3(63)	65.3(78)	60.3(71)	27.1(48)	22.3(35)	34.0(43)	30.3(37)	33.1(39)
4870(5)	68.8(65)	43.5(41)	74.5(68)	40.2(58)	58.4(56)	46.6(43)	46.3(42)	71.9(66)
5066(5)	86.7(104)	104.7(127)	89.2(106)	55.7(84)	44.2(65)	36.7(44)	28.8(34)	44.1(52)
5273(5)	100.4(73)	91.3(66)	81.3(64)	71.6(109)	52.8(49)	53.5(38)	30.5(22)	48.9(40)

window associated with p-process temperatures of the order of 3×10^9 K.

Hauser–Feshbach calculations were carried out by using the TALYS 1.6 code [29,30], which includes many different input parameter sets. Using default settings, i.e., phenomenological models for the nuclear level densities [31], γ-ray strength function [32] and optical potential [33], neither the experimental cross-section values for ground and metastable production nor the partial cross sections can be reproduced, as shown in Figs. 8 and 9.

For studying further implications of the γ-ray strength, calculations were carried out by using different level density models [31,34,35] as well as both non- [33] and semimicroscopic [36] proton optical-model potentials. Calculations using the generalized superfluid model [35] as level density differed dramatically from all other models and were excluded from further analysis. For the remaining parameter combinations, the upper and lower values for each energy are determined for a fixed γ-ray strength but with different models of nuclear level densities and optical potentials, creating theoretical uncertainty bands.

The photon transmission coefficient is most frequently described in the framework of the phenomenological Lorentzian model of the giant dipole resonance [32,35]. For nuclear astrophysics applications, it has been of particular interest to develop models of the microscopic type which are hoped to provide a reasonable reliability and predictive power for the
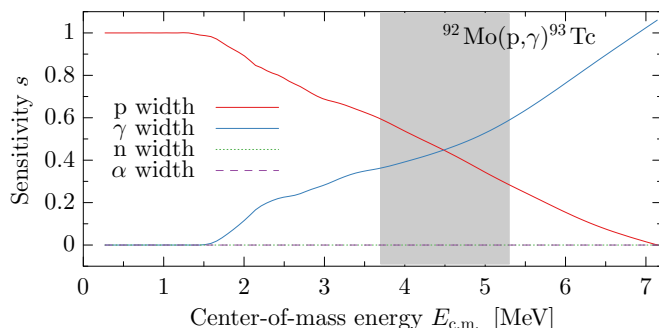
$E1$ strength function. Attempts in this direction have been conducted within the quasi-particle random-phase-approximation (QRPA) model based on realistic Skyrme or Gogny interactions. This concerns in particular the Skyrme–Hartree–Fock–Bogoliubov + QRPA (Skyrme-HFB + QRPA)model based on the BSk7 interaction [37] which also introduces
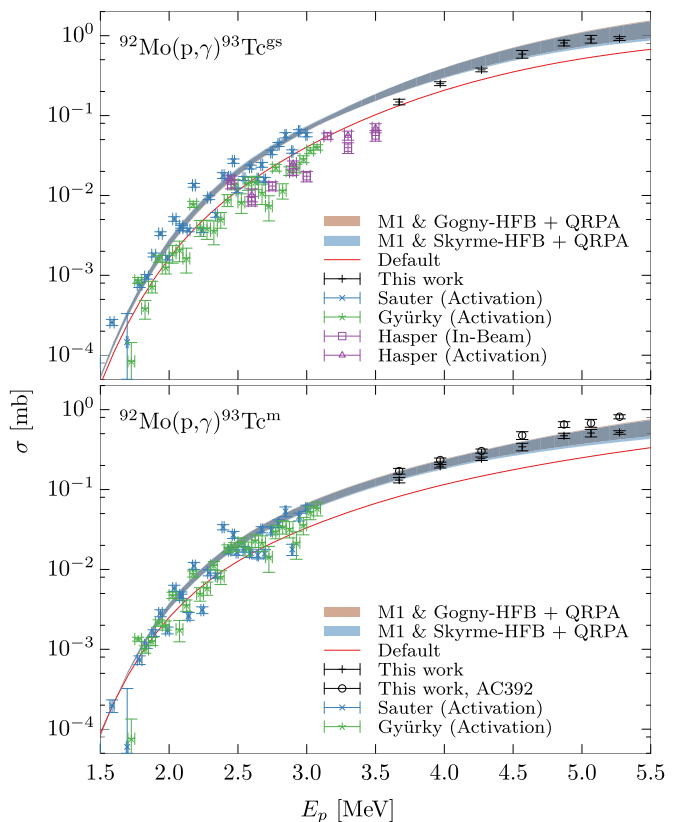

FIG. 8. Cross sections for the ^{92}Mo(p,γ)^{93}Tc reaction separated by production of the ground and metastable states of ^{93}Tc. For both, in-beam angular correlation data were obtained in this experiment. In addition, thick target activation was carried out by Sauter and Käppeler [10] as well as Gyürky *et al.* [11]. For the ground state, additional data by Hasper *et al.* [12] are available. For the metastable state, the cross section could also be obtained in this experiment by using the in-beam activation-curve method (AC392). Calculations were carried out by using TALYS; see text for details.
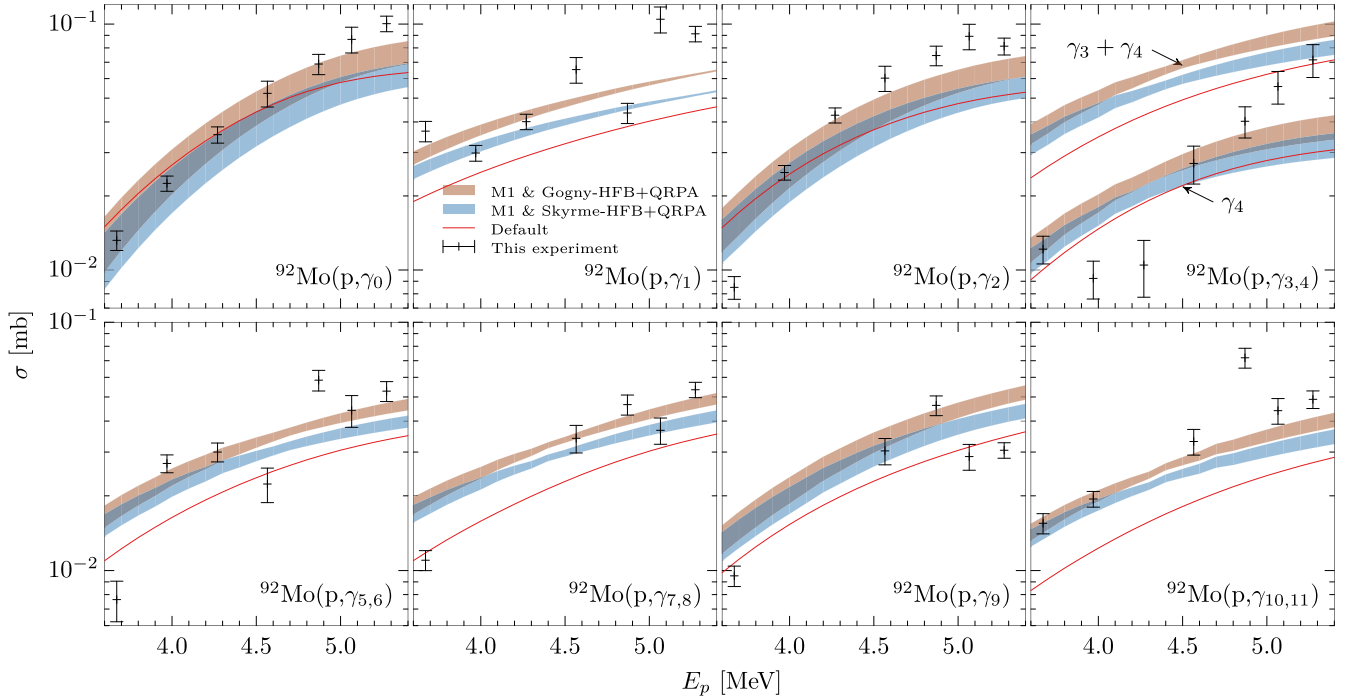

FIG. 7. Sensitivities of the ^{92}Mo(p,γ)^{93}Tc cross section when varying neutron, proton, α, and γ widths separately by a factor of two, as a function of center-of-mass energy [28]. The measured energy range is depicted by the gray shaded area.

FIG. 9. Partial cross sections for the ^{92}Mo$(p,\gamma)^{93}$Tc reaction obtained in this experiment compared with TALYS calculations; see text for details. Note that, in some cases, partial cross sections could only be determined for the sum of two transitions. These are compared with the respective sum of calculated data.

some phenomenological corrections to take the damping of the collective motion as well as the deformation effects into account. In contrast, the Gogny-HFB + QRPA model based on the D1M interaction [38] allows for a consistent description of axially symmetric deformations and includes phenomenologically the impact of phonon coupling or multiparticle-multihole configuration as a function of their densities. Both models have proven their capacity to reproduce experimental photoabsorption data relatively well [39–41].

As far as the $M1$ contribution is concerned, a shell-model calculation was performed to estimate the strength in ^{93}Tc. These calculations were performed by means of the code RITSSCHIL [42] by using a model space composed of the $\pi(0f_{5/2}, 1p_{3/2}, 1p_{1/2}, 0g_{9/2})$ proton orbits and the $\nu(1p_{1/2}, 0g_{9/2}, 1d_{5/2}, 0g_{7/2})$ neutron orbits relative to a ^{66}Ni core. This configuration space was also applied in an earlier study of $M1$ strength functions in ^{94,95,96}Mo -, ^{90}Zr - [43], and $E2$ strength functions in ^{94,95}Mo [44]. In the present calculations, three protons were allowed to be lifted from the (fp) shell to the $0g_{9/2}$ orbit and one neutron from the $0g_{9/2}$ to the $1d_{5/2}$ orbit. This resulted in dimensions up to 23 000.

The calculations included states with spins from $J = 1/2$ to $21/2$. For each spin the lowest 40 states were calculated. Reduced transition probabilities $B(M1)$ and $B(E2)$ were calculated for all transitions from initial to final states with energies $E_f < E_i$ for spins $J_f = J_i$, $J_i \pm 1$ and $J_f = J_i$, $J_i \pm 2$, respectively. For the minimum and maximum J_i, the cases $J_f = J_i - 1$ and $J_f = J_i + 1$, respectively, were excluded. This resulted in more than 24 500 $M1$ and 37 700 $E2$ transitions for each parity $\pi = +$ and $\pi = -$, which were sorted into 100 keV bins of transition energy $E_\gamma = E_i - E_f$. The average $B(M1)$

or $B(E2)$ value for one energy bin was obtained as the sum of all values divided by the number of transitions within this bin. For the spin g factors, attenuations of $g_s^{\text{eff}} = 0.7 g_s^{\text{free}}$ were applied, and for the effective charges, values of of $e_\pi = 1.5e$ and $e_\nu = 0.5e$ were used.

$M1$ strength functions were deduced from the $\overline{B}(M1)$ distributions by using the relation $f_{M1}(E_\gamma) = 16\pi/9 \ (\hbar c)^{-3} \overline{B}(M1, E_\gamma) \ \rho(E_i)$. They were calculated by multiplying the $B(M1)$ value in μ_N^2 of each transition with 11.5473×10^{-9} times the level density at the energy of the initial state $\rho(E_i)$ in MeV^{-1} and deducing averages in energy bins as done for the $\overline{B}(M1)$ values. The level densities $\rho(E_i, \pi)$ were determined by counting the calculated levels within energy intervals of 1 MeV for the two parities separately. The total level density $\rho(E_i)$ is in agreement with the constant-temperature expression $\rho(E_i) = \rho_0 \exp(E_i/T_\rho)$ for $E_i < 3$ MeV. For higher energies the combinatorial level density deviates from this expression and eventually decreases with excitation energy, which is due to missing levels at high energy in the present configuration space. From a fit to the combinatorial values in the range $E_i < 3$ MeV we obtain $\rho_0 = 1.92$ MeV^{-1} and $T_\rho = 0.76$ MeV. These values compare to our findings for the neighboring Mo isotopes [43]. The strength functions obtained for the two parities were subsequently added. $E2$ strength functions were deduced from the $\overline{B}(E2)$ distributions including all transitions in a way analogous to the one described in Ref. [44]. To calculate the $E2$ strength function the relation $f_{E2}(E_\gamma) = 0.80632 \times 10^{-12} \overline{B}(E2, E_\gamma) \ \rho(E_i)$ was used.

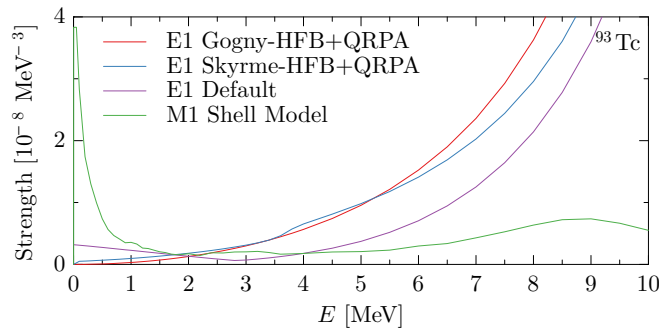The $M1$ strength function calculated for ^{93}Tc shows a low-energy enhancement similar to those found in the $N = 50$

FIG. 10. $E1$ and $M1$ γ strength in ^{93}Tc obtained by Gogny- or Skyrme-HFB + QRPA in the case of $E1$ and shell-model calculations for the case of $M1$ strength. The low-energy $M1$ strength was combined with a Lorentzian for the spin flip. See text for details.

isotone ^{90}Zr and in the neighboring isotopes ^{94,95,96}Mo [43] on the basis of analogous calculations. This low-energy enhancement of $M1$ strength explains the so-called up-bend observed in experimental dipole strength functions of nuclides in various mass regions. For the cases of ^{56,57}Fe, the large low-energy $M1$ strength was also described in the framework of the shell model [45]. Moreover, it was demonstrated that a low-energy enhancement of the dipole strength function comparable with the present one for f_{M1} has an influence on reaction rates in particular for very-neutron-rich nuclides and can increase the astrophysical (n,γ) rate of the r-process by a factor of more than 10 [46].

Adopting the Gogny- or Skyrme-HFB + QRPA E1 strength and the shell-model M1 strength (see Fig. 10) raises the cross sections significantly from the default model values, as seen in Figs. 8 and 9. This closes the gap to the experimental data at high energies, especially for the production of the metastable state. For the ground and metastable production cross sections, the difference between Gogny- and Skyrme-based calculations is minimal. Considering the partial cross sections, the Gogny-HFB + QRPA predicts slightly higher cross sections. The influence of the $E2$ strength at low energy is negligible.

With respect to the energy dependence, a split into two groups can be observed. A group with a relatively good agreement between experimental and theoretical cross sections with a soft energy dependence, including ^{93}Tc$^{\mathrm{m}}$, γ_1, and higher partial components and a group with a steeper energy dependence including ^{93}Tc$^{\mathrm{gs}}$, γ_0, γ_2, and γ_4. For the (p,γ_0) and (p,γ_2) cross sections, the high spin of the final states imply that high-multipolarity transitions only can take place between the compound state and the final state, at least at low energies where s- or p-wave protons are favored. At higher incident energies, d and f waves become efficient and consequently lower γ multipolarities start to contribute. This explains the strong energy dependence observed in the corresponding partial cross sections.

Note that, in Fig. 9, some of the partial cross sections have been added due to the overlap of the transitions. In the case of ^{92}Mo($p,\gamma_{3,4}$), the γ_3 transition should not exist, as discussed in Sec. III D. This is supported by the calculations, because the summed cross section for γ_3 and γ_4 are greatly overestimating the cross section, while the cross section for the γ_4 transition alone shows the same behavior as other partial cross sections. It is not clear where the calculated cross section for the γ_3 transition should be distributed to, since removing this state in the TALYS level scheme while keeping all other parameters constant results in only minor changes. Considering the spin dependence discussed above, a further investigation of spin and parity of this state seems desirable.

The fluctuations found in the previous thick-target activation measurements are not reproduced, as expected. Note that it was recommended by Gyürky *et al.* [11] to renormalize the Sauter and Käppeler ^{92}Mo(p,γ)^{93}Tc$^{\mathrm{gs}}$ data by a constant factor of 0.85 to account for reevaluated γ-ray transition probabilities, which leads to a better agreement of the data sets with each other. Between proton energies from 2 to 3 MeV, the production of the ground state would then, on average, be overestimated by calculations with microscopic γ strengths.

V. CONCLUSIONS

Previous measurements at lower energies have revealed an untypical fluctuating behavior of the production cross sections for the ^{92}Mo(p,γ)^{93}Tc reaction. The present measurement extends the cross-section data to higher energies from 3.7 to 5.3 MeV. Using in-beam γ-ray spectroscopy, additional partial cross sections up to the 11th state in ^{93}Tc could be acquired, which provides a fertile ground for testing γ-ray strength functions. Hauser–Feshbach theoretical calculations with TALYS using Gogny- or Skyrme-HFB + QRPA $E1$ strength and shell-model $M1$ strength show good reproduction of experimental data but are unable to reproduce all experimental features, especially at lower energies. A $\gamma\gamma$-coincidence analysis revealed a level scheme with differences from previously published data.

[1] M. Arnould and S. Goriely, Phys. Rep. **384**, 1 (2003).

[2] M. Berglund and M. E. Wieser, Pure Appl. Chem. **83**, 397 (2011).

[3] N. Dauphas, T. Rauscher, B. Marty, and L. Reisberg, Nucl. Phys. A **719**, C287 (2003).

[4] T. Rauscher, N. Dauphas, I. Dillmann, C. Fröhlich, Z. Fülöp, and G. Gyürky, Rep. Prog. Phys. **76**, 066201 (2013).

[5] M. Rayet, M. Arnould, M. Hashimoto, N. Prantzos, and K. Nomoto, Astron. Astrophys. **298**, 517 (1995).

[6] C. Travaglio, F. K. Röpke, R. Gallino, and W. Hillebrandt, Astrophys. J. **739**, 93 (2011).

[7] C. Travaglio, R. Gallino, T. Rauscher, N. Dauphas, F. K. Rpke, and W. Hillebrandt, Astrophys. J. Lett. **795**, 141 (2014).

[8] S. Goriely, J. José, M. Hernanz, M. Rayet, and M. Arnould, Astron. Astrophys. **383**, L27 (2002).

[9] W. Hauser and H. Feshbach, Phys. Rev. **87**, 366 (1952).

[10] T. Sauter and F. Käppeler, Phys. Rev. C **55**, 3127 (1997).

[11] G. Gyürky, M. Vakulenko, Z. Fülöp, Z. Halász, G. Kiss, E. Somorjai, and T. Szücs, Nucl. Phys. A **922**, 112 (2014).

[12] J. Hasper, M. Büssing, M. Elvers, J. Endres, and A. Zilges, J. Phys.: Conf. Ser. **202**, 012005 (2010).

[13] L. Netterdon, A. Endres, S. Goriely, J. Mayer, P. Scholz, M. Spieker, and A. Zilges, Phys. Lett. B **744**, 358 (2015).

[14] M. Hausmann, A. Jungclaus, E. Galindo, K. P. Lieb, O. Yordanov, I. P. Johnstone, R. Schwengner, A. Dewald, A. Fitzler, O. Möller, G. de Angelis, A. Gadea, T. Martinez, D. R. Napoli, and C. Ur, Phys. Rev. C **68**, 024309 (2003).

[15] M. Hass, C. Broude, L. Weissman, L. Müller, G. Montagnoli, F. Scarlassara, G. F. Segato, C. Signorini, G. Goldring, D. Ackermann, P. Bednarczyk, L. Corradi, P. Spolaore, M. Lindroos, S. Hormann, V. Ninov, F. P. Hessberger, F. Soramel, N. Takahashi, and B. A. Brown, Phys. Lett. B **371**, 25 (1996).

[16] G. Audi, F. Kondev, M. Wang, B. Pfeiffer, X. Sun, J. Blachot, and M. MacCormick, Chin. Phys. C **36**, 1157 (2012).

[17] H. H. Andersen, F. Besenbacher, P. Loftager, and W. Möller, Phys. Rev. A **21**, 1891 (1980).

[18] M. Mayer, AIP Conf. Proc. **475**, 541 (1999).

[19] M. Mayer, *SIMNRA Users Guide*, Tech. Rep. (Max-Planck-Institut für Plasmaphysik, Garching, 2009).

[20] J. F. Ziegler, M. Ziegler, and J. Biersack, Nucl. Instrum. Methods Phys. Res., Sect. B **268**, 1818 (2010).

[21] J. Brenneisen, D. Grathwohl, M. Lickert, R. Ott, H. Röpke, J. Schmälzlin, P. Siedle, and B. H. Wildenthal, Z. Phys. A: Hadrons Nucl. **352**, 279 (1995).

[22] L. Netterdon, V. Derya, J. Endres, C. Fransen, A. Hennig, J. Mayer, C. Müller-Gatermann, A. Sauerwein, P. Scholz, M. Spieker, and A. Zilges, Nucl. Instrum. Methods Phys. Res., Sect. A **754**, 94 (2014).

[23] B. Hubbard-Nelson, M. Momayezi, and W. K. Warburton, Nucl. Instrum. Methods Phys. Res., Sect. A **422**, 411 (1999).

[24] M.-M. Bé, V. Chechev, R. Dersch, O. Helene, R. Helmer, M. Herman, S. Hlaváč, A. Marcinkowski, G. Molnár, A. Nichols, E. Schönfeld, V. Vanin, and M. Woods, *Update of X-ray and γ-ray Decay Data Standards for Detector Calibration and other Applications* (IAEA Library, Vienna, 2007).

[25] S. Agostinelli *et al.*, Nucl. Instrum. Methods Phys. Res., Sect. A **506**, 250 (2003).

[26] C. M. Baglin, Nucl. Data Sheets **112**, 1163 (2011).

[27] R. Britton, J. Burnett, A. Davies, and P. Regan, Nucl. Instrum. Methods Phys. Res., Sect. A **769**, 20 (2015).

[28] T. Rauscher, Astrophys. J., Suppl. Ser. **201**, 26 (2012).

[29] A. J. Koning and D. Rochman, Nucl. Data Sheets **113**, 2841 (2012).

[30] A. J. Koning, S. Hilaire, and S. Goriely, *TALYS-1.6, User Manual*, Nuclear Research and Consultancy Group NRG, Petten (2013), http://www.talys.eu/fileadmin/talys/user/docs/talys1.6.pdf.

[31] A. J. Koning, S. Hilaire, and S. Goriely, Nucl. Phys. A **810**, 13 (2008).

[32] J. Kopecky and M. Uhl, Phys. Rev. C **41**, 1941 (1990).

[33] A. J. Koning and J. P. Delaroche, Nucl. Phys. A **713**, 231 (2003).

[34] S. Goriely, S. Hilaire, and A. J. Koning, Phys. Rev. C **78**, 064307 (2008).

[35] R. Capote, M. Herman, P. Oblozinsky, P. Young, S. Goriely *et al.*, Nucl. Data Sheets **110**, 3107 (2009).

[36] E. Bauge, J. P. Delaroche, and M. Girod, Phys. Rev. C **63**, 024607 (2001).

[37] S. Goriely, E. Khan, and M. Samyn, Nucl. Phys. A **739**, 331 (2004).

[38] S. Péru and M. Martini, Eur. Phys. J. A **50**, 88 (2014).

[39] T. Kondo, H. Utsunomiya, S. Goriely, C. Iwamoto, H. Akimune, T. Yamagata, H. Toyokawa, H. Harada, F. Kitatani, Y.-W. Lui, S. Hilaire, and A. Koning, Nucl. Data Sheets **119**, 310 (2014).

[40] D. M. Filipescu, I. Gheorghe, H. Utsunomiya, S. Goriely, T. Renstrøm, H.-T. Nyhus, O. Tesileanu, T. Glodariu, T. Shima, K. Takahisa, S. Miyamoto, Y.-W. Lui, S. Hilaire, S. Péru, M. Martini, and A. J. Koning, Phys. Rev. C **90**, 064616 (2014).

[41] H.-T. Nyhus, T. Renstrøm, H. Utsunomiya, S. Goriely, D. M. Filipescu, I. Gheorghe, O. Tesileanu, T. Glodariu, T. Shima, K. Takahisa, S. Miyamoto, Y.-W. Lui, S. Hilaire, S. Péru, M. Martini, L. Siess, and A. J. Koning, Phys. Rev. C **91**, 015808 (2015).

[42] D. Zwarts, Comput. Phys. Commun. **38**, 365 (1985).

[43] R. Schwengner, S. Frauendorf, and A. C. Larsen, Phys. Rev. Lett. **111**, 232504 (2013).

[44] R. Schwengner, Phys. Rev. C **90**, 064321 (2014).

[45] B. A. Brown and A. C. Larsen, Phys. Rev. Lett. **113**, 252502 (2014).

[46] A. C. Larsen and S. Goriely, Phys. Rev. C **82**, 014318 (2010).